Chemical Engineering Journal 489 (2024) 151194

Contents lists available at ScienceDirect

Chemical Engineering Journal

journal homepage: www.elsevier.com/locate/cej

Impact of mild hydrothermal aging on kinetics of NH_3, NO, SO_2 and CO oxidation reactions on Cu/SSZ-13 catalyst

Tetyana Zheleznyak [a], Petr Kočí [a,*], William Epling [b]

[a] University of Chemistry and Technology, Prague, Technická 5, Prague 166 28, Czech Republic
[b] University of Virginia, Charlottesville, 385 McCormick Rd, VA 22903, USA

ARTICLE INFO

Keywords:
SCR
Catalyst
Aging
Kinetics
Exhaust gas aftertreatment

ABSTRACT

Cu/SSZ-13 is a catalyst commonly used for selective catalytic reduction (SCR) of nitrogen oxides (NO_x) in diesel engine exhaust. Standard configurations are based on SCR preceded by an oxidation catalyst, however, a close-coupled SCR configuration appears relevant for upcoming regulations addressing cold-start emissions. Two often discussed ion-exchanged Cu sites in Cu/SSZ-13 are denoted ZCuOH and Z_2Cu, where Z represents an Al atom in the zeolite framework. Mild hydrothermal aging (HTA) causes Cu redistribution within the catalyst; ZCuOH sites transform into more stable Z_2Cu species. In this work, the effect of mild HTA on NH_3, NO, SO_2, and CO oxidation is studied on a commercial Cu/SSZ-13 sample. Temperature-programmed reaction experiments, performed in a lab reactor, and previously published catalyst characterization data using H_2-TPR, NH_3-TPD, and DRIFTS were used to build and validate a mathematical model. It couples the kinetics of the oxidation reactions with ZCuOH and Z_2Cu concentration evolution during mild HTA. The model uses two distinct rate coefficients for ZCuOH and Z_2Cu sites, allowing prediction of the catalyst activity during aging. The results suggest that the rate coefficients for the studied reactions on Z_2Cu are effectively nil, so the observed activity in NH_3, NO, SO_2, and CO oxidation can be attributed solely to ZCuOH sites.

1. Introduction

Selective catalytic reduction (SCR) is the current standard technology for abatement of nitrogen oxides (NO_x) from diesel engine vehicles exhaust and Cu/SSZ-13 catalysts are commercially used for this purpose [1–3]. The overall reaction for the standard SCR can be written as:

$$NH_3 + NO + \frac{1}{4}O_2 \longrightarrow N_2 + \frac{3}{2}H_2O \quad (1)$$

Current configurations of diesel exhaust aftertreatment systems include at least the following units: a diesel oxidation catalyst (DOC), a diesel particulate filter (DPF), an SCR catalyst, and an ammonia slip catalyst (ASC) [4]. In such a configuration, the SCR catalyst may face hydrothermal aging during regeneration of the diesel particulate filter [2,5]. Recently, in an effort to reduce cold-start emissions of NO_x, a close-coupled configuration (cc-SCR) has been proposed, where the SCR is placed directly at the outlet of the engine, upstream of the other catalyst components. This approach has been shown to effectively reduce NO_x slip due to accelerated catalyst warm-up [6–8]. However, the catalyst is exposed to higher temperatures and increased concentrations of CO, hydrocarbons, and soot, as well as SO_2, in the close-coupled configuration. Thus, the oxidation reactions that would normally take place on an upstream DOC become relevant for a close-coupled SCR catalyst and co-determine its performance. Therefore quantifying the oxidation rates over an SCR catalyst is ultimately needed to predict overall efficiency.

The Cu/SSZ-13 catalysts used for SCR have Cu ions exchanged into the structure of the SSZ-13 zeolite. Copper can be present in the catalyst in the form of mono- and multinuclear framework sites, as well as extra-framework CuO nanoparticles [9–11]. Two main framework sites are often described as present in the Cu/SSZ-13 catalyst: Z_2Cu and ZCuOH [2,3], where Z represents an Al atom in the zeolite framework. Their distribution in the catalyst depends on various factors, such as the silica-to-alumina ratio and Cu loading [12–15]. It has been shown that the Z_2Cu species is preferably populated first at lower Cu loadings, followed by ZCuOH at higher loadings [9]. Cu ions can be solvated by H_2O and NH_3, which provides these species with mobility in zeolite cages. Literature shows that the solvated species, as well as static dimers and oxygen-bridged dicopper (Cu–O–Cu) species, are prevalent in the low-temperature region, whereas at higher temperatures when H_2O and NH_3 would desorb from the catalyst, monomeric Cu bound to the zeolite has been proposed as the active SCR site [10,11,16–18].

* Corresponding author.
E-mail address: petr.koci@vscht.cz (P. Kočí).

https://doi.org/10.1016/j.cej.2024.151194
Received 7 January 2024; Received in revised form 5 April 2024; Accepted 9 April 2024
Available online 12 April 2024

Several mechanisms lead to a loss of Cu/SSZ-13 catalyst activity during its lifetime. The most important pathways are hydrothermal aging (HTA) and sulfur poisoning [1,19–23]. Sulfur poisoning is related to SO_x in the exhaust gas. The SCR catalyst performance after sulfur poisoning can be partially restored by periodic high-temperature regeneration treatment [1,24,25]. When oxygen is present in the feed, SO_2 can be oxidized to SO_3. Previous studies suggest that the extent and mechanism of sulfur poisoning on Cu/SSZ-13 by SO_2 and SO_3 is not equivalent, with more severe impact when the feed contains SO_3 [1, 25]. There is also evidence that Z_2Cu sites are less susceptible to sulfur poisoning than ZCuOH, and that the poisoning under dry conditions is strongly correlated with SO_2 oxidation on ZCuOH sites [1].

Mild hydrothermal aging leads mainly to the transformation of Cu sites [1]. In particular, the Cu ions tend to move from ZCuOH sites to more stable Z_2Cu positions, which is accompanied by a loss of Brønsted acid sites ZH [1,19,26–28]:

$$ZCuOH + ZH \longrightarrow Z_2Cu + H_2O \quad (2)$$

Temperatures above 750 °C accelerate the dealumination of the zeolite, which has a more severe impact on the zeolite structure and catalyst activity [23].

Framework Cu site distribution affects the SCR catalyst operation in several ways. Ammonia adsorption and temperature programmed desorption (TPD) experiments suggest that after mild HTA, NH_3 desorption occurs at lower temperatures, which correlates with the transformation from ZCuOH towards Z_2Cu sites by which the density of strong Brønsted acid sites decreases [2,26–29], see Eq. (2). While the SCR reaction itself seems to be independent of ZCuOH or Z_2Cu site type at low temperature, the NH_3 oxidation activity decreases with ZCuOH-to-Z_2Cu transformation during catalyst aging [1,2,22]. At high temperatures, a lower NH_3 oxidation rate was observed on aged samples and this phenomenon was shown to positively affect NO_x conversion during the stoichiometric SCR reaction, as less NH_3 was consumed in parasitic oxidation [1,2].

Recently, Khurana et al. [30] conducted a study on NO oxidation under dry conditions using Cu/SSZ-13 samples with various densities of Z_2Cu and ZCuOH species. Although neither of the monomeric sites was directly linked to the reaction, the amount of ZCuOH species affected the oxidation activity indirectly as a precursor to Cu-oxo dimers, which were identified as the active sites for NO oxidation. In contrast, the Z_2Cu site was found to be inactive in NO oxidation [12,31]. This is consistent with a study of Akter et al. [32], in which Cu/CHA samples with lower Cu loadings showed no detectable dry NO oxidation activity (due to practically all Cu sites being populated as Z_2Cu), while the samples with higher Cu loadings (containing substantial amount of ZCuOH sites) were active.

CO oxidation has been mostly studied as a titration technique for quantifying proximal ZCuOH sites and Cu dimers. Recent studies imply that at lower temperatures under dry conditions, ZCuOH sites are indirectly responsible for CO oxidation to CO_2 [30,33,34]. Iacobone et al. [33] further suggests that after adding water, both Z_2Cu and ZCuOH species are hydrolyzed and therefore active in CO_2 evolution. However, at higher temperatures, the water-mobilized species become less stable, and static Cu species become active sites for the oxidation reactions [34].

The goal of this work is to investigate the impact of mild hydrothermal aging on the steady-state kinetics of NH_3, NO, SO_2, and CO oxidation in a range of SCR operating temperatures. We compare the trends in catalytic activity for the individual reactions and identify similarities between them. We aim to develop a model that couples the Cu site transformation kinetics with the kinetics of oxidation reactions on individual Cu sites, allowing the prediction of the evolution of SCR catalyst activity during mild hydrothermal aging.

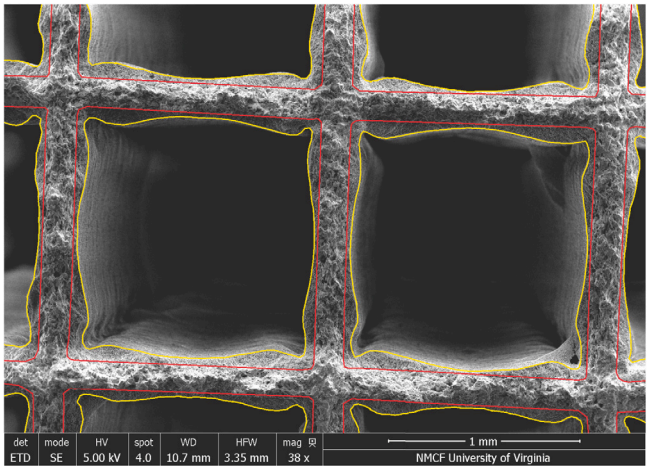

Fig. 1. Cross-section view of the Cu/SSZ-13 washcoat on monolith channels, obtained by scanning electron microscopy. Red lines indicate the substrate/coating boundaries, yellow lines mark external surface of the coated catalyst layer.

2. Experimental setup

The Cu/SSZ-13 catalyst used in the experiments was supplied by Cummins Inc and washcoated on a cordierite monolith structure with square channels and a cell density of 300 cells per square inch (cpsi). The Si:Al ratio in the SSZ-13 zeolite was 9.5 [26] and the copper loading was 3.1 wt% (484 μmol/g coating) [29]. Smaller cylindrical samples were obtained by core-drilling the original monolith; the sample geometry can be found in Table 1. The geometrical parameters for the channel and catalytic coating were evaluated from cross-section SEM image analysis, Fig. 1. Procedure used for the washcoat geometry calculation is described in detail in Supplementary Material. This ensures that the correct amount of active Cu/SSZ-13 catalyst is considered in our calculations and enables proper scaling to different catalyst loadings (e.g., other monolith configurations or catalyst powder tests).

The samples were wrapped with ceramic fiber strings and placed into a quartz tube located inside a Lindberg BlueM tube furnace with 30 cm long heated zone. The catalyst temperature was measured with K-type Omega thermocouples placed upstream and downstream of the monolith. Tubing upstream and downstream of the reactor was heated to 150 °C using heat tape, and insulated to prevent water condensation on the surface of the tubing. An FTIR MKS 2030 was used to monitor the reactor outlet concentrations of CO, CO_2, H_2O, NO, NO_2, NH_3, SO_2 and SO_3.

Before the experiments, the samples were degreened by exposing to 10% O_2, 7% H_2O, 8% CO_2 and balance N_2 at 550 °C for 4 h. This catalyst state is referred to as "degreened". The mild hydrothermal aging exposure was performed with the same gas concentrations but at 600 °C for 10 or 25 h. These hydrothermally aged samples are referred to as "HTA-600 10 h" and "HTA-600 25 h", respectively. The catalytic activity of the degreened and aged samples was tested using the selected component – 200 ppm NH_3, 200 ppm NO, 200 ppm CO, or 50 ppm SO_2 – in a mixture of 10% O_2, 8% CO_2, and 7 or 0% H_2O (wet or dry, respectively). Prior to each reaction experiment, the sample was treated in 10% O_2 at 500 °C for 1 h to ensure that Cu is oxidized to Cu^{II}. Steady-state conversions were then measured at 200, 250, 300, 350, 400, 450, 500, and 550 °C. At each temperature, the catalyst activity was stabilized for approximately 30 min to reach steady state. As will be demonstrated later in Section 4, catalyst aging during the reaction experiments was negligible compared to the HTA procedure lasting several hours at 600 °C. The total gas flow rate in all reactor experiments was 1360 cm^3/min at standard conditions, corresponding to GHSV of 62 000 h^{-1}.

Table 1
Parameters of the investigated Cu/SSZ-13 catalyst sample.

Parameter	Value
Length, L	2.9 cm
Diameter, D	0.75 cm
Channel density	320 cpsi
Channel void fraction, ε^g	0.679
Wall thickness	150 μm
Washcoat thickness	50 μm
Washcoat density, ρ_w	800 kg/m^3
Washcoat vol. fraction in solid phase, φ_w	0.361
Total Z site concentration in washcoat, Ω_Z	837 mol/m^3

The quantification of sites was adopted from Wei et al. [2] who studied the SCR reaction (1) on the same degreened and hydrothermally aged catalyst samples. NO+NH_3 temperature programmed reduction (NO+NH_3-TPR) was used to count the total amount of Cu reducible by NH_3+NO, which corresponds to the combination of ZCuOH and Z_2Cu [35–37].

After hydrothermal aging, the total amount of SCR reducible Cu did not change, which indicates that no Cu oxide particles were formed during our HTA treatments in the sample, and that the ion-exchanged ZCuOH and Z_2Cu species are responsible for any changes in Cu distribution

After hydrothermal aging, the total amount of SCR reducible Cu did not change, which indicates that no Cu oxide particles were formed during our HTA treatments in the sample and that the ion-exchanged ZCuOH and Z_2Cu species are responsible for the change in Cu distribution. Z_2Cu site density was measured by H_2-TPR experiments as proposed by Luo et al. [29]. The ZCuOH density was obtained by subtracting the amount of Z_2Cu calculated by H_2-TPR from the total reducible Cu amount obtained by the NO+NH_3-TPR experiments reported by Wei et al. [2]. Brønsted acid site (ZH) densities were calculated by the amount of NH_3 desorbed at high temperature during NH_3 temperature programmed desorption (NH_3-TPD) experiments previously published [2]. A shift from high- to low-temperature NH_3 desorption peaks correlated with the decrease of ZH site concentration that accompanies Cu transfer from ZCuOH towards Z_2Cu species.

3. Mathematical model

3.1. Transport equations

The SCR monolith sample was described using a heterogeneous 1D plug-flow model considering a coated catalyst layer on the channel wall [38–42]. The model consists of component mole balances in the flowing gas (3), inside the pores of the catalytic coating (4) and on the surface of the catalyst (5), as well as enthalpy balances of the solid phase (6) and of the flowing gas (7).

$$\frac{\partial c_k(z,t)}{\partial t} = -\frac{\partial (u\cdot c_k)}{\partial z} + \frac{k_c a}{\varepsilon^g}\, c\left(y_k^s - y_k\right), \qquad k = 1,\ldots,N_k \tag{3}$$

$$\frac{\partial c_k^s(z,t)}{\partial t} = \frac{k_c a}{\varepsilon^s(1-\varepsilon^g)\varphi_w}\, c\left(y_k - y_k^s\right) + \frac{1}{\varepsilon^s}\sum_{i=1}^{N_i} \nu_{k,i} r_i, \qquad k = 1,\ldots,N_k \tag{4}$$

$$\frac{\partial \theta_m(z,t)}{\partial t} = \frac{1}{\Omega_Z}\sum_{i=1}^{N_i} \nu_{m,i}^{\theta} r_i, \qquad m = 1,\ldots,N_m \tag{5}$$

$$\rho^s c_p^s \frac{\partial T_s(z,t)}{\partial t} = \lambda^s \frac{\partial^2 T_s}{\partial z^2} + \frac{k_h a}{1-\varepsilon^g}\left(T - T_s\right) - \varphi_w \sum_{i=1}^{N_i} \Delta H_{r,i} r_i \tag{6}$$

$$\rho c_p \frac{\partial T(z,t)}{\partial t} = -u\rho c_p \frac{\partial T}{\partial z} + \frac{k_h a}{\varepsilon^g}\left(T_s - T\right) \tag{7}$$

The partial differential equations are complemented with the following boundary conditions: (i) $c_k = c_k^{in}$ and $T = T^{in}$ at the inlet ($z = 0$), and (ii) $\partial T^s/\partial z = 0$ at both inlet and outlet ($z = 0$ and $z = L$, respectively). All the reactions considered are exothermic. Though the adiabatic increase of temperature is within 2 °C for the low reactant concentrations examined in this work, the enthalpy balances were not excluded, therefore this model is general at a negligible additional computational cost.

Table 2
Rate laws considered for NH_3, NO, SO_2 and CO oxidation reactions on Cu/SSZ-13 catalyst. The reaction rates r_i are calculated from local component mole fractions in washcoat pores y_k^s; the superscript "s" is omitted here for the sake of brevity.

	Reaction	Rate law
R_{HTA}	$ZCuOH + ZH \longrightarrow Z_2Cu + H_2O$	$r_{HTA} = k_{HTA}\exp\left(-\frac{E_{a,HTA}}{RT}\right)\theta_{ZCuOH}\,\theta_{ZH}\,\Omega_Z$
R1	$2\,NH_3 + \frac{3}{2}\,O_2 \longrightarrow N_2 + 3\,H_2O$	$r_1 = k_1\exp\left(-\frac{E_{a,1}}{RT}\right) y_{NH_3}\, y_{O_2}$
R2	$NO + \frac{1}{2}\,O_2 \longleftrightarrow NO_2$	$r_2 = k_2\exp\left(-\frac{E_{a,2}}{RT}\right)\left(y_{NO}\, y_{O_2}^{0.5} - \frac{y_{NO_2}}{K_2^{eq}}\right)$
R3	$SO_2 + \frac{1}{2}\,O_2 \longleftrightarrow SO_3$	$r_3 = k_3\exp\left(-\frac{E_{a,3}}{RT}\right)\left(y_{SO_2}\, y_{O_2}^{0.5} - \frac{y_{SO_3}}{K_3^{eq}}\right)$
R4	$CO + \frac{1}{2}\,O_2 \longrightarrow CO_2$	$r_4 = k_4\exp\left(-\frac{E_{a,4}}{RT}\right) y_{CO}\, y_{O_2}$

The mass (k_c) and heat (k_h) transfer coefficients' profiles along the monolith channel are calculated using correlations proposed by Ramanathan et al. [43]. The numerical solution of the partial differential equations is obtained by the finite difference method with 20 spatial discretization intervals using a semi-implicit integration scheme with quasi-linearization of reaction rates, implemented in Fortran.

3.2. Reaction kinetics

The reaction kinetics are incorporated into the model equations through reaction rates r_i, see the right-hand sides of Eqs. (4), (5), and (6). Thus, the reaction terms r_i affect concentrations of gas and surface components, including Cu sites speciation. The considered reactions and their rate laws r_i are listed in Table 2.

The kinetics of Cu site transformations during mild hydrothermal aging (HTA) of Cu/SSZ-13 catalyst is considered first order in ZCuOH as well as in Brønsted acid sites ZH, see reaction R_{HTA} in Table 2. The aging rate law is in agreement with the aging kinetics model proposed by Daya et al. [27]. The total number of Z sites (i.e., Al atoms in the zeolite framework) remains constant during mild hydrothermal aging:

$$1 = \theta_{ZCuOH} + \theta_{Z_2Cu} + \theta_{ZH} \tag{8}$$

Note that the dimensionless site concentrations θ_{ZCuOH}, θ_{Z_2Cu} and θ_{ZH} are normalized by Ω_Z, which is the total concentration of Z sites present in the zeolite (moles of sites per volume of catalytic coating). The calculation takes into account the number of Z sites present in each species. Thus, the concentration of Cu sites in the form of ZCuOH can be expressed as $\theta_{ZCuOH}\,\Omega_Z$ and in the form of Z_2Cu as $\frac{1}{2}\theta_{Z_2Cu}\,\Omega_Z$. The concentration of framework Cu sites is assumed constant:

$$\theta_{ZCuOH} + \frac{1}{2}\theta_{Z_2Cu} = \text{constant} \tag{9}$$

The kinetic parameters for Cu site transformation during mild hydrothermal aging were evaluated from ZCuOH and Z_2Cu site concentrations measured in the degreened and aged catalyst sample by the characterization techniques described in Section 2.

The employed steady-state reaction kinetics of NH_3, NO, SO_2, and CO oxidation are listed in Table 2. NO and SO_2 oxidation may become limited by thermodynamic equilibrium, while NH_3 and CO oxidation are practically irreversible in the studied range of temperatures. The reaction i takes place on ZCuOH and Z_2Cu sites with different rates and the overall pre-exponential factor k_i is obtained as a combination reflecting individual Cu site concentrations:

$$k_i = k_{i,ZCuOH}\,\theta_{ZCuOH}^n\,\Omega_Z + k_{i,Z_2Cu}\,\frac{1}{2}\theta_{Z_2Cu}^n\,\Omega_Z \tag{10}$$

As can be seen in Table 2, the activation energy was considered site-independent because the slope of conversion-vs-temperature curves

measured with the degreened and aged catalyst sample did not change significantly.

The proposed scaling of catalyst activity with the number of sites does not depend on a particular rate limiting step (adsorption, surface reaction, or desorption). On the other hand, the number of sites involved in the reaction (single vs. dual Cu site mechanism) might affect the dependence on the site concentration. It has been reported that the low-temperature SCR mechanism involves mobile Cu dimers [16], which leads to 2nd order in Cu site concentration [37]. The role of Cu dimers was reported and confirmed at lower temperatures (below 250 °C), mainly in the presence of water and/or ammonia that solvate and mobilize Cu ions. It is known that another reaction mechanism evolves on Cu/SSZ-13 at higher temperatures [44]. Our work covers a wide range of operating temperatures up to 550 °C and a significant steady-state conversion of NO, CO, SO_2 and NH_3 is achieved only above 250 °C. Thus, the impact of the low-temperature mechanism on our results is minor. Furthermore, 1st order in Cu site concentration is expected for oxidation reactions involving Eley-Rideal mechanism on single atom catalysts [45]. Thus, we first performed computations assuming 1st order in Cu site concentration using $n = 1$ in Eq. (10). Subsequently, we repeated the simulations considering 2nd order in Cu site concentration using $n = 2$ in Eq. (10) and compared the results of both approaches.

The kinetic parameters for individual sites were evaluated by minimizing the differences between the measured and simulated outlet concentrations of the key component k in the given reaction (NH_3, NO, CO or SO_2), considering a set of data points j at temperatures 200–550 °C. The least-squares approach was employed, defining the objective function S as:

$$S = \sum_{j=1}^{N_j} \left(y_{k,j}^{\text{sim}} - y_{k,j}^{\text{exp}} \right)^2 \tag{11}$$

A simplex method [46] was used for minimization of the objective function S individually for each reaction. The procedure included the following steps. (i) Using the measured data for the degreened sample, optimum activation energy $E_{a,i}$ was found together with an overall pre-exponential factor k_i. (ii) The complete set of experimental data including both degreened and aged samples that differed in ZCuOH and Z_2Cu site densities was then used for evaluation of pre-exponential factors $k_{i,\text{ZCuOH}}$ and k_{i,Z_2Cu}, employing equation (10). In this second step, the previously obtained activation energy $E_{a,i}$ was already fixed. Furthermore, a binding condition was used that enforced the values of $k_{i,\text{ZCuOH}}$ and k_{i,Z_2Cu} to provide the same overall pre-exponential factor k_i for the degreened catalyst as obtained in the first step.

In the following text, the results obtained with rate coefficient k_i decomposed to $k_{i,\text{ZCuOH}}$ and k_{i,Z_2Cu} according to Eq. (10), utilizing the actual site densities θ_{ZCuOH} and θ_{Z_2Cu} predicted by the hydrothermal aging kinetics r_{HTA}, Table 2, will be denoted as "predicted". These results were further compared to the "best fit" obtained with a single-parameter fitting of effective rate coefficient k_i^{eff} directly to the data measured for the aged samples. Thus, the k_i^{eff} represents the best possible fit for the given catalyst state independent of site concentrations, while equation (10) predicts the reaction rate from the actual ZCuOH and Z_2Cu site fractions.

4. Results

The simulated ZCuOH and Z_2Cu concentration evolution during mild hydrothermal aging is shown in Fig. 2. A simultaneous decrease in ZCuOH and an increase in Z_2Cu sites is predicted with hydrothermal aging time. The simulation results are in good agreement with the experimental data obtained by characterization techniques discussed in Section 2, see the black crosses in Fig. 2. The corresponding values of site fractions in the degreened state and after 10 and 25 h of aging are summarized in Table 3.

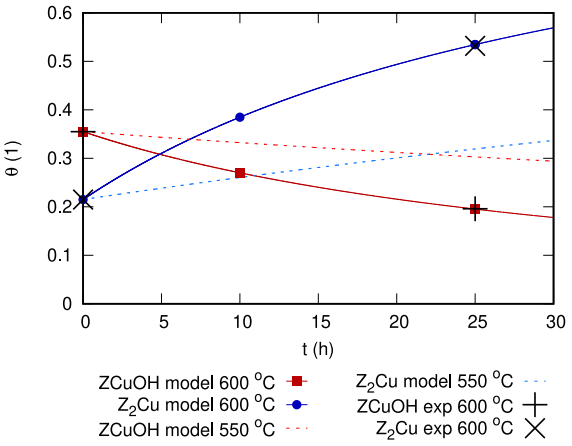

Fig. 2. Fractions of ZCuOH and Z_2Cu sites during hydrothermal aging of the Cu/SSZ-13 catalyst sample at 600 °C (solid line) and 550 °C (dashed line) as predicted by the HTA model. Colored points mark the catalyst states examined in this work and black crosses experimental data from catalyst characterization.

Table 3
Concentrations of active sites at different stages of hydrothermal aging as predicted by the model.

HTA time (h)	0	10	25
Coverages normalized by Ω_Z			
θ_{ZCuOH} (–)	0.355	0.272	0.194
θ_{Z_2Cu} (–)	0.215	0.380	0.536
θ_{ZH} (–)	0.430	0.348	0.270
Site concentrations per washcoat volume			
Cu as ZCuOH (mol/m^3)	297	228	163
Cu as Z_2Cu (mol/m^3)	90	159	224
Brønsted sites ZH (mol/m^3)	360	291	226

As already mentioned, the concentration of Cu sites in the form of Z_2Cu is $\frac{1}{2}\theta_{Z_2Cu}\,\Omega_Z$ because θ_{Z_2Cu} is based on the number of Z sites involved. The rate coefficient for Cu migration during hydrothermal aging at 600 °C is 1.98×10^{-5} s^{-1}. Considering the activation energy $E_{a,\text{HTA}} = 175$ kJ/mol proposed by Daya et al. [27] for a similar type of Cu/SSZ-13 catalyst, our HTA rate corresponds to the pre-exponential factor $k_{\text{HTA}} = 5.85 \times 10^5$ s^{-1}. For comparison, Daya et al. [27] reported pre-exponential factor $k_{\text{HTA}} = 5.09 \times 10^5$ s^{-1}, which is close to the k_{HTA} value obtained from our characterization data.

Fig. 2 also shows the evolution of ZCuOH and Z_2Cu site concentrations at 550 °C as predicted by the HTA model, considering the activation energy $E_{a,\text{HTA}} = 175$ kJ/mol [27]. Note that 550 °C was the maximum temperature reached only for the last 30 min during the reaction experiments. Thus, the catalyst aging during the reaction experiments was negligible compared to the HTA procedure lasting 10 or 25 h at 600 °C.

After identification of the aging kinetics and quantification of ZCuOH and Z_2Cu sites, we focused on the kinetics of NH_3, NO, SO_2 and CO oxidation over the degreened and hydrothermally aged samples. The kinetic parameters of individual reactions were evaluated using two approaches. The first approach used two independent pre-exponential factors for ZCuOH and Z_2Cu sites, Eq. (10), enabling predictions of the aged catalyst activity based on the actual site concentrations. We started with the 1st-order dependence on site density ($n = 1$) and then tested also the 2nd-order ($n = 2$) in Eq. (10) for comparison. The second approach aimed on the identification of an effective pre-exponential factor that provides the best fit of the experimental data at the given aging state, independent of the actual site concentrations.

Fig. 3 shows the results of experiments and simulations for NH_3 oxidation on the degreened, 10 h, and 25 h aged samples. Almost no reaction is observed at 200 °C. With increasing temperature, the outlet

Table 4
Evaluated kinetic parameters for the studied oxidation reactions considering 1st-order dependence on ZCuOH and Z_2Cu site concentrations, $n = 1$ in Eq. (10).

Reaction	Conditions	$k_{i,ZCuOH}$ (s^{-1})	k_{i,Z_2Cu} (s^{-1})	$k_i^{degreened}$ ($mol\,m^{-3}\,s^{-1}$)	$E_{a,i}$ ($kJ\,mol^{-1}$)
R1 (NH_3)	wet	1.67×10^7	0	5.26×10^9	63.9
R2 (NO)	wet	1.56×10^4	0	4.64×10^6	41.4
R3 (SO_2)	dry	1.71×10^3	0	5.08×10^5	29.1
R4 (CO)	wet	1.09×10^8	0	3.24×10^{10}	80.0
R4 (CO)	dry	1.42×10^7	0	4.22×10^9	64.9

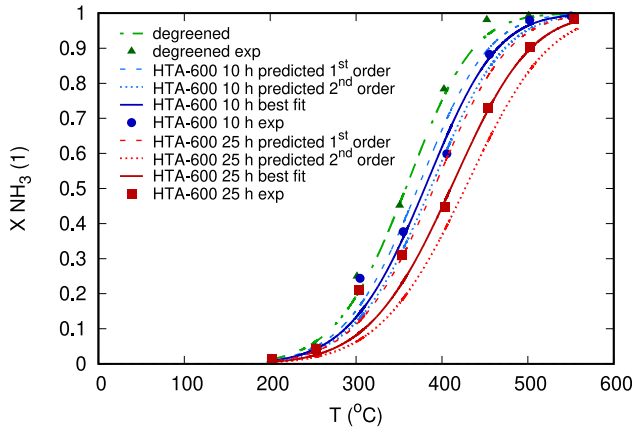

Fig. 3. Steady-state conversions during NH_3 oxidation on the degreened and hydrothermally aged (HTA) Cu/SSZ-13 catalyst, wet conditions. Points — experimental data, dashed lines — simulation results with the rate coefficient k_i depending on θ_{ZCuOH} predicted by the HTA model, solid lines — the best fit with an effective rate coefficient k_i^{eff}.

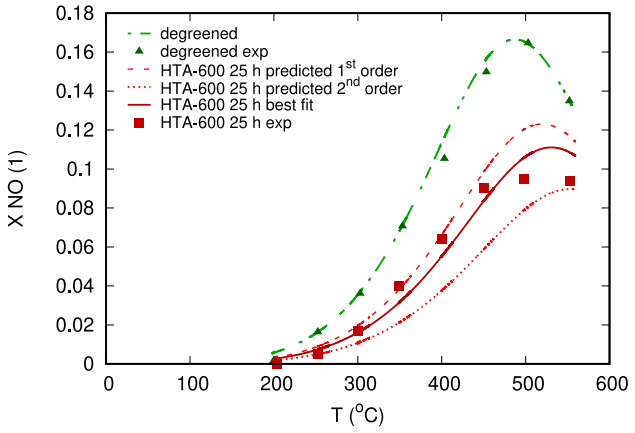

Fig. 4. Steady-state conversions during NO oxidation on the degreened and hydrothermally aged (HTA) Cu/SSZ-13 catalyst, wet conditions. Points — experimental data, dashed lines — simulation results with the rate coefficient k_i depending on θ_{ZCuOH} predicted by the HTA model, solid lines — the best fit with an effective rate coefficient k_i^{eff}.

NH_3 conversion gradually increases due to increasing reaction rate. The degreened catalyst exhibits the highest extent of NH_3 oxidation. Catalytic activity decreases for the 10 h and 25 h aged samples, resulting in lower outlet NH_3 conversions. The simulated curves match the trends observed in experiments. For the 10 h aged sample, the 1st-order prediction based on ZCuOH and Z_2Cu site concentrations (dashed curve in Fig. 3) provides results close to the best possible fit of the experimental data (solid curve in Fig. 3). For the 25 h aged sample, the deviation between the 1st-order predictive approach and the best fit of the measured data points increases — the actual activity is slightly lower than predicted. Nevertheless, the prediction based on ZCuOH and Z_2Cu site concentrations is still reasonably good.

The evaluated kinetic parameters in Table 4 reveal that zero pre-exponential factor of NH_3 oxidation on Z_2Cu sites is identified by the optimization method for the 1st-order dependence in Eq. (10), suggesting that the catalyst activity is correlated just to the concentration of ZCuOH sites. Note, the value of zero for the parameter k_{i,Z_2Cu} is obtained when the optimization method only allows the parameter value to reach this physically meaningful limit. Formally, it would be possible to achieve results closer to the best fit in Fig. 3 if there was a negative contribution of Z_2Cu sites in the 1st-order predictive model, but obviously this is not physically meaningful. Thus, the interpretation of the obtained results is: the decrease in catalytic activity observed in experiments corresponds to, and even slightly exceeds, the loss of ZCuOH sites in the tested sample. The remaining rows of Table 4 indicate that the same conclusion can also be made for the NO, SO_2, and CO oxidation reactions.

Considering the identified value of $k_{i,Z_2Cu} = 0$, Eq. (10) simplifies to:

$$k_i = k_{i,ZCuOH}\,\theta_{ZCuOH}^{n}\,\Omega_Z \tag{12}$$

so that the reaction rate coefficients effectively depend only on ZCuOH site concentration. As already explained, mild hydrothermal aging does not affect significantly the concentration of Z sites in the zeolite structure, hence Ω_Z is constant. The intrinsic rate coefficient on ZCuOH site $k_{i,ZCuOH}$ remains constant as well. When equation (12) for the aged catalyst is divided by the same equation using the parameters of the degreened catalyst, a simple formula is obtained that can be used for the k_i^{aged} prediction:

$$\frac{k_i^{aged}}{k_i^{degreened}} = \left(\frac{\theta_{ZCuOH}^{aged}}{\theta_{ZCuOH}^{degreened}}\right)^n \tag{13}$$

To test if the 2nd-order dependence on Cu site concentration reported at lower temperatures [37] is relevant for the studied reactions in a broad temperature range examined in this work, we repeated the simulations using $n = 2$ in Eq. (13). The NH_3 conversion curves predicted by a 2nd-order model go below the measured data, see the dotted lines in Fig. 3. This indicates that the loss of catalytic activity observed in the experiment is lower than would correspond to the 2nd-order dependence on ZCuOH site concentration. However, the 2nd-order predictions are a bit closer to the best fit compared to the 1st-order predictions. The corresponding root mean square errors (RMSE) for the simulated NH_3 conversions in Fig. 3 are provided in Supplementary Material, Table S1.

The measured and simulated outlet conversions during NO oxidation are depicted in Fig. 4. Note that the NO oxidation rate becomes limited by reaction equilibrium above ca. 450 °C and the outlet NO conversion decreases at temperatures above 500 °C, which is captured correctly by the model for both the degreened and aged samples. The loss of NO oxidation activity predicted for the aged sample using the 1st-order dependence on ZCuOH site concentration (dashed line) is very close to the best possible fit of the measured data (solid line). In contrast, the 2nd-order prediction results in conversions that are too low, overestimating the catalyst deactivation for NO oxidation. The corresponding root mean square errors for the simulated NO conversions in Fig. 4 are provided in Supplementary Material, Table S2.

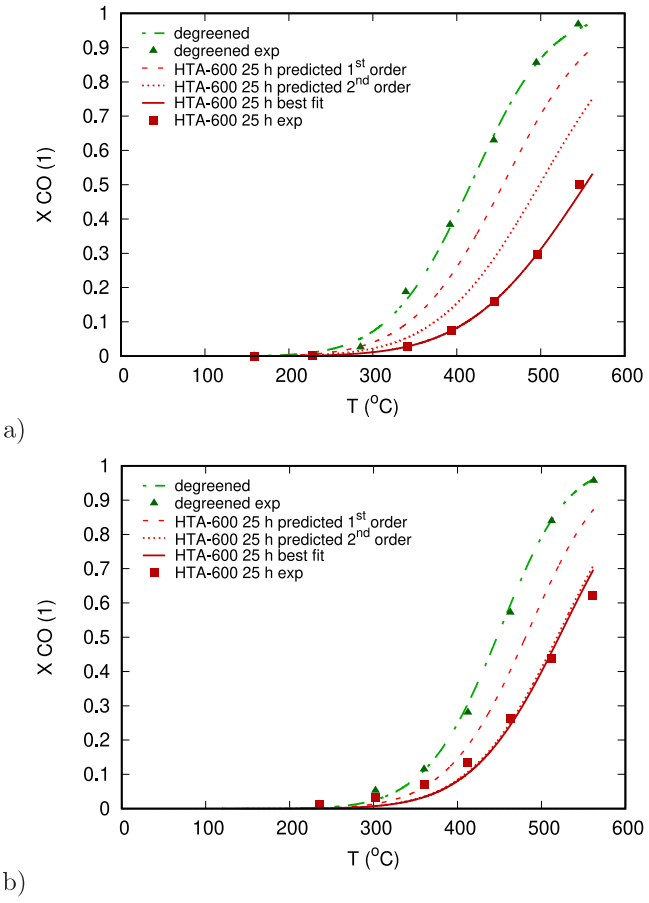

Fig. 5. Steady-state conversions during CO oxidation under (a) dry and (b) wet conditions on the degreened and hydrothermally aged (HTA) Cu/SSZ-13 catalyst. Points — experimental data, dashed lines — simulation results with the rate coefficient k_i depending on θ_{ZCuOH} predicted by the HTA model, solid lines — the best fit with an effective rate coefficient k_i^{eff}.

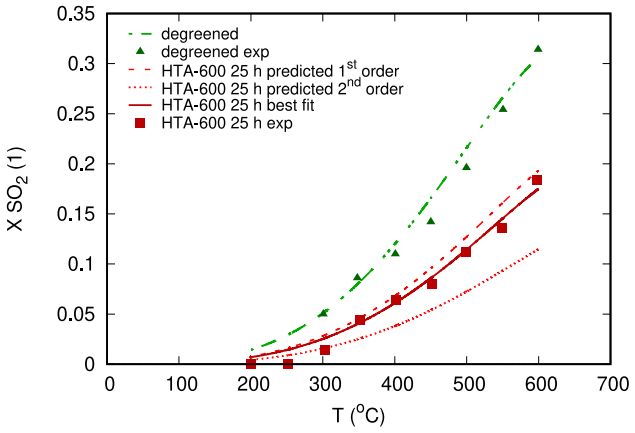

Fig. 6. Steady-state conversions during SO_2 oxidation on the degreened and hydrothermally aged (HTA) Cu/SSZ-13 catalyst, dry conditions. Points — experimental data, dashed lines — simulation results with the rate coefficient k_i depending on θ_{ZCuOH} predicted by the HTA model, solid lines — the best fit with an effective rate coefficient k_i^{eff}.

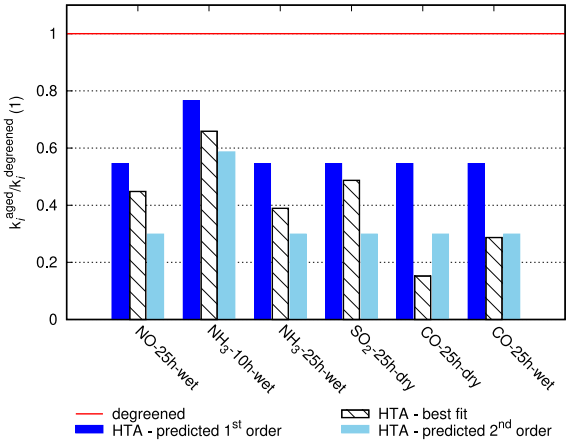

Fig. 7. Relative rate coefficients $k_i^{aged}/k_i^{degreened}$ as predicted by the hydrothermal aging model using 1st or 2nd order in ZCuOH (dark and light blue bars, respectively) and obtained by the best fit of the measured data (hatched bars). All the values are normalized by the corresponding rate coefficient on the degreened sample $k_i^{degreened}$ (red line as a reference).

CO oxidation was examined both in dry (0% H_2O) and wet (7% H_2O) conditions, Fig. 5. It can be seen that the presence of water affects the CO oxidation rate to a different extent on the degreened and aged samples. The degreened sample exhibits somewhat lower activation energy under dry conditions (the corresponding E_a values are provided in Table 4), but the aged sample performs better under wet conditions, Fig. 5a,b. Ambivalent effects of water depending on structural parameters of the zeolite cages were already reported for the low-temperature SCR reaction [47]. Water effects on the reaction kinetics may include both inhibition and promotion, which requires additional characterization of the catalyst structure and more detailed reaction mechanisms to be addressed in future studies. We can only speculate that water inhibits CO oxidation at lower-to-intermediate temperatures but acts as a CO oxidant at high temperatures, which would explain the behavior observed in Fig. 5a,b. For CO oxidation, the predictions using a 2nd-order dependence on ZCuOH site concentration match the experimental results much better than the 1st-order predictions. Under wet conditions, Fig. 5b, the 2nd-order prediction is practically identical with the best possible fit. For dry conditions, the measured outlet conversion is lower than predicted, which means that even the 2nd-order model underestimated the actual loss in catalytic activity. The corresponding root mean square errors for the simulated CO conversions in Fig. 5 are provided in Supplementary Material, Table S3.

SO_2 oxidation results under dry conditions are plotted in Fig. 6. The corresponding experiment under wet conditions was not performed due to extensive SO_x adsorption, formation of H_2SO_4, extremely long times needed to reach steady state due to acid formation and inconsistency in closing the mass balance due to FTIR cell limitations. Similar to NO oxidation, SO_2 oxidation can be potentially limited by thermodynamic equilibrium at high conversions and increased temperatures. However, this limitation plays only a minor role under the studied range of operating conditions; just the last temperature point is slightly affected. The decrease in SO_2 oxidation rate on the aged sample predicted by the 1st-order model depending on the changes in ZCuOH sites concentration matches the measured data and is practically identical to the best possible fit, see the red dashed and solid line in Fig. 6. The 2nd-order predictions overestimate aging impact on SO_2 conversions, see the red dotted line in Fig. 6. The corresponding root mean square errors for the simulated SO_2 conversions in Fig. 6 are provided in Supplementary Material, Table S4.

Table 5 and Fig. 7 provide a summary comparison of predicted and fitted rate coefficients k_i for NH_3, NO, SO_2, and CO oxidation for the hydrothermally aged samples. Note that all k_i values in Fig. 7 are normalized by the corresponding rate coefficient on the degreened sample, see $k_i^{degreened}$ in Table 4. The "best fit" values closely reflect

Table 5
Overall pre-exponential factors for the catalyst hydrothermally aged at 600 °C: k_i predicted by Eq. (13), using 1st-order (n = 1) or 2nd-order (n = 2) in ZCuOH site concentrations, compared to k_i^{eff} fitted directly to the measured data (best fit).

Reaction	Conditions	Aging (h)	Predicted 1st order k_i (mol m^{-3} s^{-1})	Predicted 2nd order k_i (mol m^{-3} s^{-1})	Best fit k_i^{eff} (mol m^{-3} s^{-1})
R1 (NH_3)	wet	10	4.03×10^9	3.08×10^9	3.59×10^9
R1 (NH_3)	wet	25	2.87×10^9	1.57×10^9	2.13×10^9
R2 (NO)	wet	25	2.53×10^6	1.38×10^6	2.23×10^6
R3 (SO_2)	dry	25	2.78×10^5	1.52×10^5	2.71×10^5
R4 (CO)	wet	25	1.77×10^{10}	9.67×10^9	9.31×10^9
R4 (CO)	dry	25	2.31×10^9	1.26×10^9	6.42×10^8

the measured reaction rates, while the predicted values relate the rate coefficients to the actual concentration of ZCuOH sites, see Eq. (13) and Table 3. Direct comparison of the predicted rate coefficients k_i to the best fitted k_i^{eff} in Table 5 reveals how appropriate the correlation between ZCuOH and the rate coefficient is. Additional measures in terms of root mean square error are provided in Supplementary Material, Tables S1–S4. The predictive model assuming 1st-order dependence on ZCuOH site density is very close to the best fit for NO and SO_2 oxidation. The 1st-order prediction is less accurate in case of NH_3 oxidation, but still usable. Both 1st-order and 2nd-order provide comparable accuracy for NH_3 oxidation and the obtained results do not allow clear discrimination between them. The only case that is clearly better described by the 2nd-order dependence on ZCuOH site concentration is CO oxidation, where the reaction rate observed experimentally on the aged catalyst is noticeably lower than the 1st-order prediction.

5. Conclusions

The developed kinetic model includes the gradual transformation of ZCuOH sites into Z_2Cu during mild hydrothermal aging of a Cu/SSZ-13 catalyst and its impact on NH_3, NO, SO_2, and CO oxidation rates in a broad range of temperatures. The combined experimental and modeling results suggest negligible rates of the studied reactions on Z_2Cu sites and a close correlation of the overall reaction rates to the concentration of ZCuOH sites, which is of 1st order for NO, NH_3 and SO_2 oxidation, while CO oxidation exhibits a 2nd-order dependence. The model provides a reasonably accurate prediction of the aged catalyst's activities for NH_3, NO, SO_2, and CO oxidation reactions as the reactions follow similar trends with mild hydrothermal aging. The proposed coupling of Cu site transformation kinetics with the kinetics of oxidation reactions provides a powerful tool for predictive simulations of SCR catalyst performance in terms of changes with time and under realistic operating conditions. In particular, the changes in NH_3 oxidation rates are crucial for precise urea dosing and SO_2 oxidation represents a key step in the sulfur poisoning mechanism, and all reactions are important to consider for close-coupled SCR configurations.

Nomenclature

a	momentum flux correction factor, 1
c_p	heat capacity, J kg^{-1} K^{-1}
c	molar concentration, mol m^{-3}
D	diameter, m
E_a	activation energy, J mol^{-1}
$_4H_r$	reaction enthalpy, J mol^{-1}
k_i	pre-exponential factor of rate coefficient for reaction i, s^{-1}
k_{HTA}	pre-exponential factor of hydrothermal aging rate, s^{-1}
k_c	mass transfer coefficient, m s^{-1}
k_h	heat transfer coefficient, J s^{-1} m^{-2} K^{-1}
L	length, m
n	order in Cu sites, 1
N	total number of elements in a set, 1
R	universal gas constant, J mol^{-1} K^{-1}
r_i	reaction rate per volume of catalytic washcoat, mol s^{-1} m^{-3}
S	sum of squares, 1
T	temperature, K
t	time variable
u	linear velocity, m s^{-1}
y	molar fraction, 1
z	spatial coordinate
Greek letters	
ϵ	porosity, 1
λ	heat conductivity, W m^{-1} K^{-1}
ν	stoichiometric coefficient, 1
φ_w	volume fraction of catalytic washcoat in solid phase, 1
ρ	density, kg m^{-3}
θ	surface site coverage, 1
Ω_Z	aluminum site concentration in zeolite framework, mol m^{-3} washcoat
Subscripts and superscripts	
eff	effective
exp	measured (experimental)
g	gas
i	index of reaction
in	inlet
j	index of measured data point
k	index of gas component
m	index of surface component
out	outlet
s	solid
w	catalytic washcoat
Z	aluminum site in zeolite framework
Abbreviations	
ASC	ammonia slip catalyst
cc-SCR	close coupled selective catalytic reduction of NO_x
cpsi	channels per square inch
DOC	diesel oxidation catalyst
DPF	diesel particulate filter
DRIFTS	diffuse reflectance infrared Fourier-transform spectroscopy
FTIR	Fourier-transform infrared spectroscopy
GHSV	gas hourly space velocity
HTA	hydrothermal aging
RMSE	root mean square error
SCR	selective catalytic reduction of NO_x
SEM	scanning electron microscopy
TPD	temperature programmed desorption
TPR	temperature programmed reduction

CRediT authorship contribution statement

Tetyana Zheleznyak: Writing – original draft, Visualization, Software, Investigation. **Petr Kočí:** Writing – review & editing, Supervision, Software, Methodology, Funding acquisition, Conceptualization. **William Epling:** Writing – review & editing, Supervision, Methodology, Funding acquisition, Conceptualization.

Declaration of competing interest

The authors declare that they have no known competing financial interests or personal relationships that could have appeared to influence the work reported in this paper.

Data availability

Data will be made available on request.

Acknowledgments

The work was financially supported by the Czech Science Foundation, Czech Republic (GACR 23-07137L) and the National Science Foundation, United States (NSF 2227016).

Appendix A. Supplementary data

Supplementary material related to this article can be found online at https://doi.org/10.1016/j.cej.2024.151194.

References

[1] Y.-R. Chen, L. Wei, A. Kumar, D. Wang, W.S. Epling, How changes in Cu-SSZ-13 catalytic oxidation activity via mild hydrothermal aging influence sulfur poisoning extents, Catal. Sci. Technol. 12 (2022) 6891–6902, http://dx.doi.org/10.1039/D2CY01394K.

[2] L. Wei, Y.-R. Chen, S. Marino, Y. Gu, W.S. Epling, Kinetic modeling of NH_3-selective catalytic reduction (SCR) over a mildly hydrothermally aged commercial Cu-SSZ-13 catalyst, Chem. Eng. J. 467 (2023) 143318, http://dx.doi.org/10.1016/j.cej.2023.143318.

[3] A.J. Shih, J.M. González, I. Khurana, L.P. Ramírez, A. Peña L., A. Kumar, A.L. Villa, Influence of ZCuOH, Z_2Cu, and extraframework Cu_xO_y species in Cu-SSZ-13 on N_2O formation during the selective catalytic reduction of NOx with NH_3, ACS Catal. 11 (16) (2021) 10362–10376, http://dx.doi.org/10.1021/acscatal.1c01871.

[4] T.V. Johnson, Review of selective catalytic reduction (SCR) and related technologies for mobile applications, in: I. Nova, E. Tronconi (Eds.), Urea-SCR Technology for DeNOx After Treatment of Diesel Exhausts, Springer New York, New York, NY, 2014, pp. 3–31.

[5] D. Wang, J. Cao, P. Tan, Z. Wang, W. Li, Z. Liu, J. Wang, Full course evolution characteristics of DPF active regeneration under different inlet HC concentrations, Fuel 310 (2022) 122452, http://dx.doi.org/10.1016/j.fuel.2021.122452.

[6] Q. Zhao, J. Li, A. Jiao, F. Liu, H. Xu, X. Liao, Pollutant emission characteristics of the close-coupled selective catalytic reduction system for diesel engines under low exhaust temperature conditions, Fuel 354 (2023) 129303, http://dx.doi.org/10.1016/j.fuel.2023.129303.

[7] L. Shiyu, W. Boyuan, G. Zexian, W. Buyu, Z. Zhaohuan, M. Xiao, C. Chen-Teng, W. Peng, H. Xin, S. Xingyu, S. Shijin, Experimental investigation of urea injection strategy for close-coupled SCR aftertreatment system to meet ultra-low NOx emission regulation, Appl. Therm. Eng. 205 (2022) 117994, http://dx.doi.org/10.1016/j.applthermaleng.2021.117994.

[8] M. Börnhorst, O. Deutschmann, Advances and challenges of ammonia delivery by urea-water sprays in SCR systems, Prog. Energy Combust. Sci. 87 (2021) 100949, http://dx.doi.org/10.1016/j.pecs.2021.100949.

[9] C. Paolucci, A.A. Parekh, I. Khurana, J.R. Di Iorio, H. Li, J.D. Albarracin Caballero, A.J. Shih, T. Anggara, W.N. Delgass, J.T. Miller, F.H. Ribeiro, R. Gounder, W.F. Schneider, Catalysis in a cage: Condition-dependent speciation and dynamics of exchanged Cu cations in SSZ-13 zeolites, J. Am. Chem. Soc. 138 (18) (2016) 6028–6048, http://dx.doi.org/10.1021/jacs.6b02651.

[10] Y. Zhang, J. Zhang, H. Wang, W. Yang, C. Wang, Y. Peng, J. Chen, J. Li, F. Gao, Selective catalytic reduction of NOx with NH_3 over Cu/SSZ-13: Elucidating dynamics of Cu active sites with in situ UV–Vis spectroscopy and DFT calculations, J. Phys. Chem. C 126 (20) (2022) 8720–8733, http://dx.doi.org/10.1021/acs.jpcc.2c01268.

[11] F. Gao, E.D. Walter, M. Kollár, Y. Wang, J. Szanyi, C.H. Peden, Understanding ammonia selective catalytic reduction kinetics over Cu/SSZ-13 from motion of the Cu ions, J. Catalysis 319 (2014) 1–14, http://dx.doi.org/10.1016/j.jcat.2014.08.010.

[12] F. Gao, N.M. Washton, Y. Wang, M. Kollár, J. Szanyi, C.H. Peden, Effects of Si/Al ratio on Cu/SSZ-13 NH_3-SCR catalysts: Implications for the active Cu species and the roles of Brønsted acidity, J. Catalysis 331 (2015) 25–38, http://dx.doi.org/10.1016/j.jcat.2015.08.004.

[13] S.A. Bates, A.A. Verma, C. Paolucci, A.A. Parekh, T. Anggara, A. Yezerets, W.F. Schneider, J.T. Miller, W.N. Delgass, F.H. Ribeiro, Identification of the active Cu site in standard selective catalytic reduction with ammonia on Cu-SSZ-13, J. Catalysis 312 (2014) 87–97, http://dx.doi.org/10.1016/j.jcat.2014.01.004.

[14] C. Paolucci, A.A. Verma, S.A. Bates, V.F. Kispersky, J.T. Miller, R. Gounder, W.N. Delgass, F.H. Ribeiro, W.F. Schneider, Isolation of the copper redox steps in the standard selective catalytic reduction on Cu-SSZ-13, Angew. Chem. Int. Ed. 53 (44) (2014) 11828–11833, http://dx.doi.org/10.1002/anie.201407030.

[15] J. Kwak, D. Tran, J. Szanyi, C. Peden, J. Lee, The effect of copper loading on the selective catalytic reduction of nitric oxide by ammonia over Cu-SSZ-13, Catal. Lett. 142 (2012) http://dx.doi.org/10.1007/s10562-012-0771-y.

[16] C. Paolucci, I. Khurana, A.A. Parekh, S. Li, A.J. Shih, H. Li, J.R. Di Iorio, J.D. Albarracin-Caballero, A. Yezerets, J.T. Miller, W.N. Delgass, F.H. Ribeiro, W.F. Schneider, R. Gounder, Dynamic multinuclear sites formed by mobilized copper ions in NO_x selective catalytic reduction, Science 357 (6354) (2017) 898–903, http://dx.doi.org/10.1126/science.aan5630.

[17] C. Negri, T. Selleri, E. Borfecchia, A. Martini, K.A. Lomachenko, T.V.W. Janssens, M. Cutini, S. Bordiga, G. Berlier, Structure and reactivity of oxygen-bridged diamino dicopper(II) complexes in Cu-ion-exchanged chabazite catalyst for NH_3-mediated selective catalytic reduction, J. Am. Chem. Soc. 142 (37) (2020) 15884–15896, http://dx.doi.org/10.1021/jacs.0c06270.

[18] C. Liu, H. Kubota, T. Amada, K. Kon, T. Toyao, Z. Maeno, K. Ueda, J. Ohyama, A. Satsuma, T. Tanigawa, N. Tsunoji, T. Sano, K.-i. Shimizu, In situ spectroscopic studies on the redox cycle of NH_3-SCR over Cu-CHA zeolites, ChemCatChem 12 (11) (2020) 3050–3059, http://dx.doi.org/10.1002/cctc.202000024.

[19] Y. Xi, C. Su, N.A. Ottinger, Z.G. Liu, Effects of hydrothermal aging on the sulfur poisoning of a Cu-SSZ-13 SCR catalyst, Appl. Catal. B 284 (2021) 119749, http://dx.doi.org/10.1016/j.apcatb.2020.119749.

[20] H. Jiang, B. Guan, X. Peng, Y. Wei, R. Zhan, H. Lin, Z. Huang, Effect of sulfur poisoning on the performance and active sites of Cu/SSZ-13 catalyst, Chem. Eng. Sci. 226 (2020) 115855, http://dx.doi.org/10.1016/j.ces.2020.115855.

[21] P.S. Hammershøi, Y. Jangjou, W.S. Epling, A.D. Jensen, T.V. Janssens, Reversible and irreversible deactivation of Cu-CHA NH_3-SCR catalysts by SO_2 and SO_3, Appl. Catal. B 226 (2018) 38–45, http://dx.doi.org/10.1016/j.apcatb.2017.12.018.

[22] J. Luo, D. Wang, A. Kumar, J. Li, K. Kamasamudram, N. Currier, A. Yezerets, Identification of two types of Cu sites in Cu/SSZ-13 and their unique responses to hydrothermal aging and sulfur poisoning, Catal. Today 267 (2016) 3–9, http://dx.doi.org/10.1016/j.cattod.2015.12.002.

[23] D. Wang, Y. Jangjou, Y. Liu, M.K. Sharma, J. Luo, J. Li, K. Kamasamudram, W.S. Epling, A comparison of hydrothermal aging effects on NH_3-SCR of NO_x over Cu-SSZ-13 and Cu-SAPO-34 catalysts, Appl. Catal. B 165 (2015) 438–445, http://dx.doi.org/10.1016/j.apcatb.2014.10.020.

[24] L. Zhang, D. Wang, Y. Liu, K. Kamasamudram, J. Li, W. Epling, SO_2 poisoning impact on the NH_3-SCR reaction over a commercial Cu-SAPO-34 SCR catalyst, Appl. Catal. B 156–157 (2014) 371–377, http://dx.doi.org/10.1016/j.apcatb.2014.03.030.

[25] A. Kumar, M.A. Smith, K. Kamasamudram, N.W. Currier, H. An, A. Yezerets, Impact of different forms of feed sulfur on small-pore Cu-zeolite SCR catalyst, Catal. Today 231 (2014) 75–82, http://dx.doi.org/10.1016/j.cattod.2013.12.038.

[26] R. Daya, S.Y. Joshi, J. Luo, R.K. Dadi, N.W. Currier, A. Yezerets, On kinetic modeling of change in active sites upon hydrothermal aging of Cu-SSZ-13, Appl. Catal. B 263 (2020) 118368, http://dx.doi.org/10.1016/j.apcatb.2019.118368.

[27] R. Daya, D. Trandal, R.K. Dadi, H. Li, S.Y. Joshi, J. Luo, A. Kumar, A. Yezerets, Kinetics and thermodynamics of ammonia solvation on Z_2Cu, ZCuOH and ZCu sites in Cu-SSZ-13 – Implications for hydrothermal aging, Appl. Catal. B 297 (2021) 120444, http://dx.doi.org/10.1016/j.apcatb.2021.120444.

[28] R. Daya, D. Trandal, U. Menon, D.J. Deka, W.P. Partridge, S.Y. Joshi, Kinetic model for the reduction of Cu^{II} sites by NO + NH_3 and reoxidation of NH_3-solvated Cu^{I} sites by O_2 and NO in Cu-SSZ-13, ACS Catal. 12 (11) (2022) 6418–6433, http://dx.doi.org/10.1021/acscatal.2c01076.

[29] J. Luo, F. Gao, K. Kamasamudram, N. Currier, C.H. Peden, A. Yezerets, New insights into Cu/SSZ-13 SCR catalyst acidity. Part I: Nature of acidic sites probed by NH_3 titration, J. Catalysis 348 (2017) 291–299, http://dx.doi.org/10.1016/j.jcat.2017.02.025.

[30] I. Khurana, J.D. Albarracin-Caballero, A.J. Shih, Identification and quantification of multinuclear Cu active sites derived from monomeric Cu moieties for dry NO oxidation over Cu-SSZ-13, J. Catalysis 413 (2022) 1111–1122, http://dx.doi.org/10.1016/j.jcat.2022.08.005.

[31] A.A. Verma, S.A. Bates, T. Anggara, C. Paolucci, A.A. Parekh, K. Kamasamudram, A. Yezerets, J.T. Miller, W.N. Delgass, W.F. Schneider, F.H. Ribeiro, NO oxidation: A probe reaction on Cu-SSZ-13, J. Catalysis 312 (2014) 179–190, http://dx.doi.org/10.1016/j.jcat.2014.01.017.

[32] N. Akter, X. Chen, J. Parise, J. Boscoboinik, T. Kim, Effects of copper loading on NH_3-SCR and NO oxidation over Cu impregnated CHA zeolite, Korean J. Chem. Eng. 35 (2017) http://dx.doi.org/10.1007/s11814-017-0268-x.

[33] U. Iacobone, I. Nova, E. Tronconi, R. Villamaina, M. Ruggeri, J. Collier, D. Thompsett, Transient CO oxidation as a versatile technique to investigate Cu titration, speciation and sites hydrolysis on Cu–CHA catalysts: The Cu loading effect, Top. Catalysis 66 (2023) 1–10, http://dx.doi.org/10.1007/s11244-023-01813-8.

[34] C. Paolucci, J.R. Di Iorio, W.F. Schneider, R. Gounder, Solvation and mobilization of copper active sites in zeolites by ammonia: Consequences for the catalytic reduction of nitrogen oxides, Acc. Chem. Res. 53 (9) (2020) 1881–1892, http://dx.doi.org/10.1021/acs.accounts.0c00328.

[35] P.S. Hammershøi, C. Negri, G. Berlier, S. Bordiga, P. Beato, T.V.W. Janssens, Temperature-programmed reduction with NO as a characterization of active Cu in Cu-CHA catalysts for NH_3-SCR, Catal. Sci. Technol. 9 (2019) 2608–2619, http://dx.doi.org/10.1039/C9CY00358D.

[36] R. Villamaina, S. Liu, I. Nova, E. Tronconi, M.P. Ruggeri, J. Collier, A. York, D. Thompsett, Speciation of Cu cations in Cu-CHA catalysts for NH_3-SCR: Effects of SiO_2/AlO_3 ratio and Cu-loading investigated by transient response methods, ACS Catal. 9 (10) (2019) 8916–8927, http://dx.doi.org/10.1021/acscatal.9b02578.

[37] F. Gramigni, N.D. Nasello, N. Usberti, U. Iacobone, T. Selleri, W. Hu, S. Liu, X. Gao, I. Nova, E. Tronconi, Transient kinetic analysis of low-temperature NH_3-SCR over Cu-CHA catalysts reveals a quadratic dependence of Cu reduction rates on Cu^{II}, ACS Catal. 11 (8) (2021) 4821–4831, http://dx.doi.org/10.1021/acscatal.0c05362.

[38] P. Kočí, M. Marek, M. Kubíček, T. Maunula, M. Härkönen, Modelling of catalytic monolith converters with low- and high-temperature NO_x storage compounds and differentiated washcoat, Chem. Eng. J. 97 (2) (2004) 131–139, http://dx.doi.org/10.1016/S1385-8947(03)00151-7.

[39] A. Güthenke, D. Chatterjee, M. Weibel, B. Krutzsch, P. Kočí, M. Marek, I. Nova, E. Tronconi, Current status of modeling lean exhaust gas aftertreatment catalysts, in: G. Marin (Ed.), Automotive Emission Control, in: Advances in Chemical Engineering, vol. 33, Academic Press, 2007, pp. 103–283, http://dx.doi.org/10.1016/S0065-2377(07)33003-2.

[40] D. Chatterjee, P. Kočí, V. Schmeißer, M. Marek, M. Weibel, B. Krutzsch, Modelling of a combined NO_x storage and NH_3-SCR catalytic system for Diesel exhaust gas aftertreatment, Catal. Today 151 (3) (2010) 395–409, http://dx.doi.org/10.1016/j.cattod.2010.01.014.

[41] M. Leskovjan, P. Kočí, T. Maunula, Simulation of diesel exhaust aftertreatment system DOC—pipe—SCR: The effects of Pt loading, PtO_x formation and pipe configuration on the deNO_x performance, Chem. Eng. Sci. 189 (2018) 179–190, http://dx.doi.org/10.1016/j.ces.2018.05.031.

[42] A. Buzková Arvajová, P. Boutikos, R. Pečinka, P. Kočí, Global kinetic model of NO oxidation on Pd/γ-Al_2O_3 catalyst including PdO_x formation and reduction by CO and C_3H_6, Appl. Catal. B 260 (2020) 118141, http://dx.doi.org/10.1016/j.apcatb.2019.118141.

[43] K. Ramanathan, V. Balakotaiah, D.H. West, Light-off criterion and transient analysis of catalytic monoliths, Chem. Eng. Sci. 58 (8) (2003) 1381–1405, http://dx.doi.org/10.1016/S0009-2509(02)00679-6.

[44] P.S. Dhillon, M.P. Harold, D. Wang, A. Kumar, S.Y. Joshi, Modeling and analysis of transport and reaction in washcoated monoliths: Cu-SSZ-13 SCR and dual-layer Cu-SSZ-13+Pt/Al_2O_3 ASC, React. Chem. Eng. 4 (2019) 1103–1115, http://dx.doi.org/10.1039/c8re00325d.

[45] W. Yang, Y. Feng, X. Chen, C. Wu, F. Wang, Z. Gao, Y. Liu, X. Ding, H. Li, Understanding trends in the NO oxidation activity of single-atom catalysts, J. Environ. Chem. Eng. 10 (2022) 108744, http://dx.doi.org/10.1016/j.jece.2022.108744.

[46] J.A. Nelder, R. Mead, A simplex method for function minimization, Comput. J. 7 (1965) 308–313, http://dx.doi.org/10.1093/comjnl/7.4.308.

[47] N.D. Nasello, U. Iacobone, N. Usberti, A. Gjetja, I. Nova, E. Tronconi, R. Villamaina, M.P. Ruggeri, D. Bounechada, A.P.E. York, J. Collier, Investigation of Low-Temperature OHC and RHC in NH_3–SCR over Cu-CHA Catalysts: Effects of H_2O and SAR, ACS Catal. 14 (2024) 4265–4276, http://dx.doi.org/10.1021/acscatal.4c00118.